Supporting information for: Ketorolac beats Ketoprofen: lower photodecarboxylation, photohemolysis and phototoxicity

Christopher D. McTiernan, Chiara Fasciani, María González-Béjar, Daniel Roca-Sanjuán, Emilio I. Alarcon, and José Carlos Netto-Ferreira

MATERIALS AND METHODS

Materials: Ketorolac tromethamine was purchased from Sigma Aldrich and used as received or in its acidic form. NaCl, NaH_2PO_4, Na_2HPO_4, dichloromethane, phenalenone, benzophenone, 1-methylnaphthalene, 1,4-cyclohexadiene, 2-propanol, tryptophan methyl ester, tyrosine methyl ester, 2`-deoxyguanosine (>99%) and tolmetin were purchased from Sigma-Aldrich. Phenyl(1*H*-pyrrol-2-yl)methanone (2-benzoylpyrrole) was obtained from Maybridge (part of Thermo Fisher Scientific).

Synthesis and characterization of 5-benzoyl-2,3-dihydro-1H-pyrrolizine-1-carboxylic acid methyl ester (Ketorolac ester): To a dry methanolic solution of Ketorolac acid (50 mg, 0.19 mmol) under nitrogen at room temperature, thionyl chloride (10 mL, 138 mmol) was added and heated under reflux, under vigorous stirring, for 14 h. After, the solvent was removed and the residue was treated with 10% NaOH (2 x 15 mL) and extracted with ethyl acetate (3 x 10 mL). The combined organic fractions were washed with saturated aqueous sodium bicarbonate (2 x 10 mL), and water (10 mL). The organic solution was dried with anhydrous Na_2SO_4, filtered, and evaporated. The residual yellow oil was purified via column chromatography (SiO_2, ethyl acetate/hexane (2:1; *v/v*)) to yield 5-benzoyl-2,3-dihydro-1H-pyrrolizine-1-carboxylic acid methyl ester (38.5 mg, 0.14 mmol, 73%). The NMR signals match literature reports.[1] $C_{16}H_{15}NO_3$:^{1}H-NMR (400 MHz, $CDCl_3$) δ 2.76-2.96 (m, 2H), 3.77 (s, 3H), 4.08 (m, 1H), 4.41-4.48 (m, 1H), 4.54-4.61 (m, 1H), 6.10 (d, 1H, *J*=4 Hz), 6.82 (d, 1H, *J*=4 Hz), 7.43 (m, 3H), 7.80 (s, 1H), 7.82 (s, 1H). ^{13}C-NMR (100 MHz, $CDCl_3$): δ 30.6 (s), 42.1 (s), 47.2 (s), 52.2 (s), 102.8 (s), 124.6 (s), 126.8 (s), 127.8 (d), 128.5 (d), 131.0 (s), 138.9 (s), 142.0 (s), 171.9 (s), 184.7 (s).

Synthesis and characterization of 5-benzoyl-1,2-dihydro-3H-pyrrolo[1,2a]pyrrole (Ketorolac decarboxylation product): A saturated solution of Ketorolac trometamine in acetonitrile (250 mL) under nitrogen at room temperature was irradiated with 8 UVB lamps in a pyrex round bottom flask in a LZC4V-Luzchem photoreactor. The solvent was evaporated and chloroform and an acidic solution were added to the solid. After separation of the two phases, anhydrous $MgSO_4$ was added to the organic part, and solvent was evaporated after filtration. The solid was dissolved in $CDCl_3$ and analyzed by ^{1}H-NMR. The NMR signals match literature reports and only the decarboxylated product was observed.[3] $C_{14}H_{13}NO$: ^{1}H-NMR (400 MHz, $CDCl_3$) δ 2.55-2.87 (m, 4H), 4.74 (t, 2H), 5.92-6.79 (m, 2H), 7.42-7.50 (m, 3H), 7.79 (m, 2H).

Absorbance measurements: Absorption spectra were recorded using a Cary-100 UV-Visible spectrophotometer (Palo Alto, CA, USA) equipped with a 1.0 cm cell holder. All measurements were recorded at room temperature unless otherwise indicated.

PHOTOTOXICITY ASSAY

The phototoxicity of several NSAIDs and their photodecomposition products were evaluated *in vitro* on human dermal fibroblasts at low passage number (between 1 and 5). The fibroblasts were grown in Dulbecco's modified eagle's medium (DMEM, Gibco) containing 10% fetal calf serum (Invitrogen) and penicillin/streptomycin (Lonza Walkersville), and cultured at 37 °C, 5.0% CO_2 in a humidified incubator. Phototoxicity was evaluated by using CellTiter96® Aqueous MTS (3-(4,5-dimethyl-2-tiazol)-2,5-diphenil-2*H*-tetrazolium bromide; tiazol blue) colorimetric viability assay (Promega) and employed as a measure of cell survival. Briefly, from a confluent cell culture, 5 x 10^4 cells/mL (cell counting was carried out using the trypan blue exclusion method) were

seeded into 96-well plates, after which different dilutions of the NSAIDs and their corresponding photodecomposition products were added before a 14 h incubation period. The plate was organized in such a way that each of the drugs was tested in triplicate and at three different concentrations (1, 10, and 100 μM). The plates also contained control wells, to which no drug was added, or to which only different concentrations of DMSO (0.1, 1.0, and 10.0%) were added to account for the fact that the different solutions were prepared through dilution of a DMSO stock solution using DMEM supplemented with fetal calf serum. The wells were also loaded in such a way that the left and right half the plates are identical, allowing for one of the sides to be covered with aluminum foil to prevent UVA exposure. Following the 14 h incubation period, each of the wells were washed with 200 μL of fresh media to ensure removal of any trace of the drugs which were not up taken by the cells. The contents of the wells were then replaced with 100 μL of fresh media. There were 6 plates labeled P1-P6. Plates P1 and P4 were control plates and were not exposed to UVA light and were analyzed by MTS assay immediately after the 14 h incubation and 24 h after the initial 14 h incubation, respectively. The other plates were irradiated for either 2 or 4 h in a 37 °C, 5.0% CO_2 humidified incubator, using a Luzchem Expo panel fitted with 5 UVA lamps (51915.7 mW/m^2). Plates P2 and P3 were analyzed immediately after 2 h and 4 h irradiations; whereas plate P5 and P6 were analyzed 24 h after 2 h and 4 h irradiations, respectively. The MTS assays were performed by the addition of 20 μL of MTS solution to each of the wells followed by incubation in a 37 °C, 5.0% CO_2 humidified incubator for 1 h. The absorbance was then recorded at 490 nm in a Victor well pate reader, at 20 °C.

PHOTOHEMOLYSIS ASSAY

Freshly drawn blood was obtained from Mr. Christopher McTiernan. To isolate the erythrocytes, the sample was diluted 10 fold with PBS and centrifuged 3x at 2500 rpm for 15 minutes. After each centrifugation, the supernatant was carefully removed and discarded, while the remaining solution was resuspended in PBS.

The erythrocyte suspension was then diluted with PBS so that the optical density of the solution was between 0.4-0.8 at 650 nm. An OD of 0.5 corresponds to 3.3×10^6 cells/ml.

The hemolysis was determined by measuring the decreasing OD at 650 nm. This is due to the fact that it has been reported that the optical density at 650 nm is linearly proportional to the amount of intact red blood cells. The drugs and their corresponding decarboxylated photoproducts were added to the suspensions as solutions in DMSO. The percentage of DMSO in the final solution is less than 1% in all cases. The hemolysis experiments were conducted at 10, 30, and 60 μM of the compounds. The results are the average of triplicate experiments. In each case the solutions were UVA irradiated as 4mL samples in quartz test tubes. The irradiation of the samples was conducted using a Luzchem photoreactor fitted with 14 UVA (81197.4 mW/m^2) bulbs and a sample carousel. The temperature inside the reactor was kept at 25°C for the duration of the experiment. The samples were irradiated for 15 minutes and then left in the dark for 1 hour prior to analysis. As controls samples containing no compound and the various concentrations of compound were kept in the dark for the same amount of time before analysis. A control was also performed to ensure that DMSO itself does not induce hemolysis. In all cases minimal to no hemolysis was seen in the controls. The 100% hemolysed sample was prepared through sonication of a suspension of RBC in PBS.

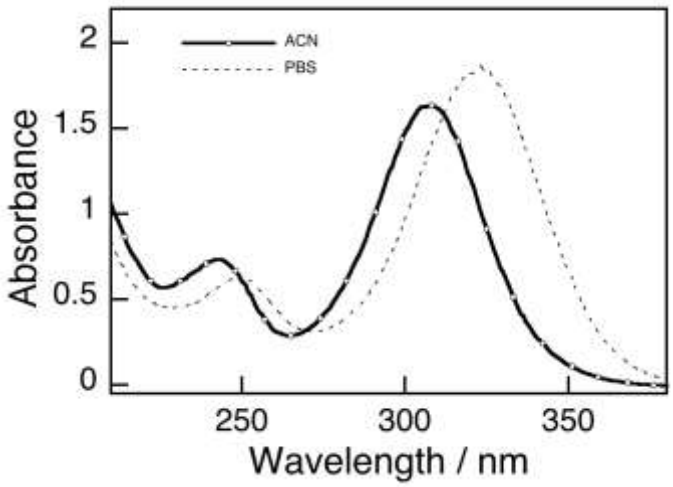

Figure S1. Ketorolac UV-Visible spectra in acetonitrile (black line) or in 100 mM phosphate buffer pH 7.0 (dashed line).

THEORETICAL METHODS AND ANALYSES

Computational details. The present theoretical analyses were carried out by using the DFT and CASSCF/CASPT2 methods as implemented in the Gaussian 09[4] and MOLCAS 7.6[5] quantum-chemical packages of software, respectively. The B3LYP hybrid density functional and both 6-31G(*d*,*p*) and 6-31+G(*d*,*p*) basis sets were employed in the DFT calculations. In particular, DFT geometry optimizations were performed at the B3LYP/6-31G(*d*,*p*) level of theory and at the optimized structures energies were computed at the B3LYP/6-31+G(*d*,*p*) level, namely the B3LYP/6-31+G(*d*,*p*)//6-31G(*d*,*p*) approach. Within the multiconfigurational CASSCF/CASPT2 calculations, the basis sets of atomic natural orbital ANO-S and ANO-L contracted to C,N,O [3s,2p,1d]/H [2s1p] and to C,N,O [4s3p1d]/H[2s1p] (hereafter ANO-S 321/21 and ANO-L 431/21, respectively).[6] While ground-state geometry optimizations were carried out at the CASSCF/ANO-S 321/21 level of theory, the structure of the lowest singlet excited state was optimized with the largest basis set (CASSCF/ANO-L 431/21 level).

Energies were calculated at the CASPT2/ANO-L 431/21 level. These approaches will be called CASPT2/ANO-L 431/21//CASSCF/ANO-S 321/21 and CASPT2//CASSCF/ANO-L 431/21, respectively. An active space of 12 electrons in 12 orbitals was employed in the CASSCF/CASPT2 calculations of the $\pi \rightarrow \pi^*$ states [CASSCF/CASPT2(12-in-12)], which comprises all the π orbitals in the benzene, carbonyl, and pyrrole groups except the all-in-phase π orbital in the benzene moiety (see Figure S2 for an illustration of the orbital shapes).

In some cases, the later orbital was also included in the active space, resulting in the CASSCF/CASPT2(14-in-13) level. For the characterization of the $n \rightarrow \pi^*$ states the

oxygen lone pair; n_O in the C_3O_1 moiety (see Fig. S3 for atom labeling) was treated in addition as active orbital together with the whole π-system [CASSCF/CASPT2(16-in-14) approach]. In CASPT2 calculations, the core orbitals of non-hydrogen atoms were not correlated, an imaginary level-shift of 0.2 a.u., was turn on a priori to minimize weakly interacting intruder states, and the non-standard IPEA modification of the zeroth-order Hamiltonian with a value of 0.00 a.u. was employed. The effect of polar solvents in the computed gas-phase properties was studied throughout the analysis of the dipole moments for ground and excited states or alternatively means polarized continuum model (PCM).

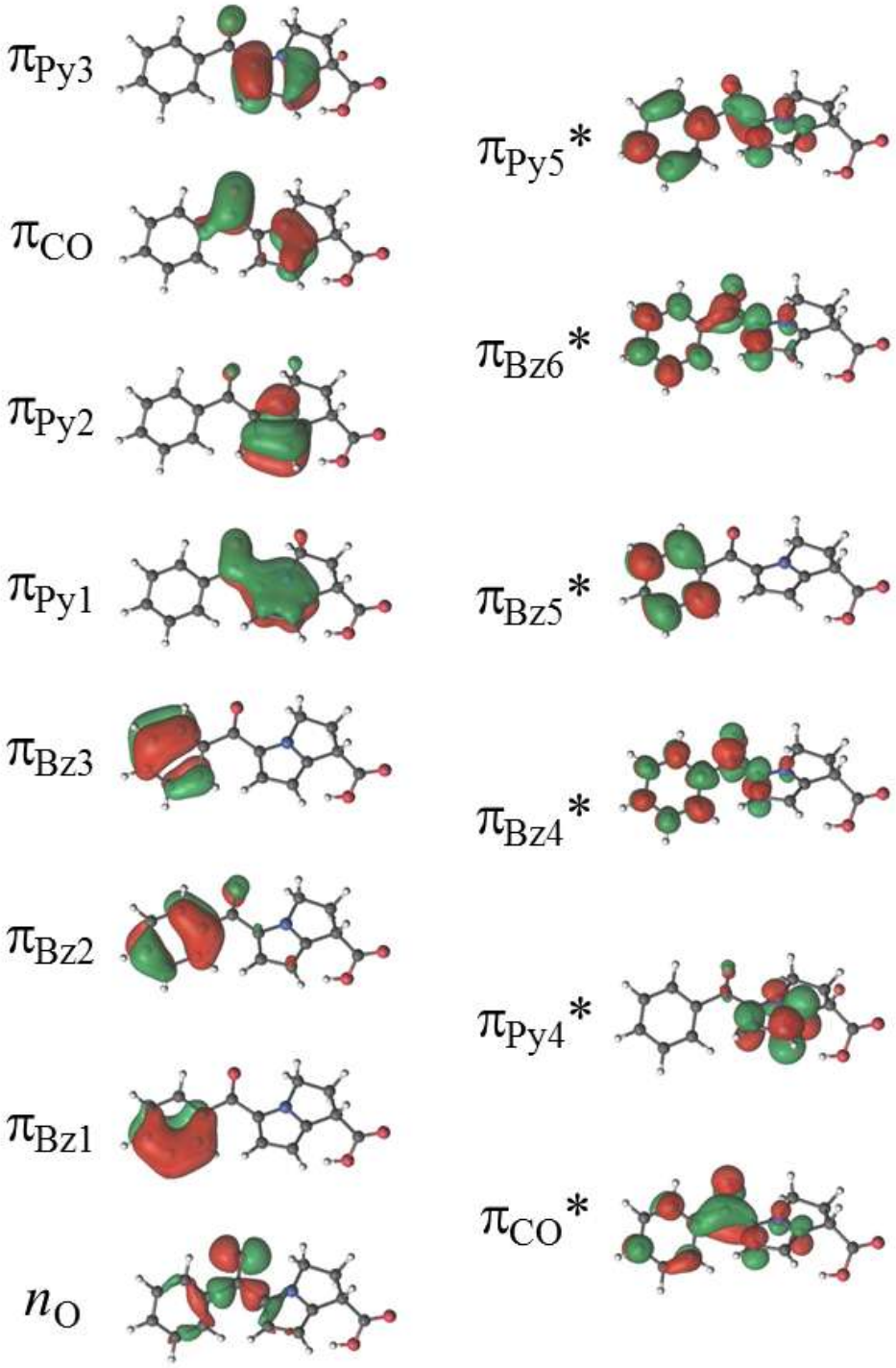

Figure S2. Molecular orbitals employed as active orbitals in the CASSCF/CASPT2(16-in-14) computations of ketorolac. The lone pair of the oxygen atom n_O is kept inactive in the CASSCF/CASPT2(14-in-13) calculations and the CASSCF/CASPT2(12-in-12) computations employ, in the active space, all the orbitals except n_O and the all-in-phase π_{Bz1} orbital.

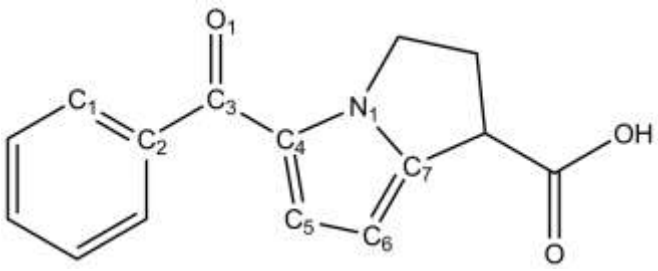

Figure S3. Ketorolac structure and atom labeling.

Conformational analysis, solvent effects and absorption spectrum. Variations in the $O_1C_3C_4N_1$ dihedral angle of ketorolac (see Fig. S3) can originate two isomers *cis* and *trans* where the *cis* isomer is around 4.5 kcal/mol, in the gas phase, more stable than the *trans* form (see Figure S4). However, computational calculations reveal that in acetonitrile both isomers are stabilized by ~10 kcal/mol maintaining a similar relative energy difference as *in-vacuo* (see Table S1). According to these relative energies, equilibrium between both forms is expected at room temperature placing the *cis* isomer around 3.6 kcal/mol lower than the *trans*. Thus, our theoretical studies will be mainly focused on the *cis* form (in some cases the *trans* isomer has been also included).

Table S1. Solvent effects in the stability of the ground-state *cis* and *trans* ketorolac isomers. Energies (in kcal/mol) relative to the cis isomer in vacuo and to the *cis* in acetonitrile (in parenthesis).

	In vacuo	Acetonitrile
Cis	0.00	-9.11 (0.00)
Trans	4.48	-5.53 (3.58)

Table S2 compiles the low-energy absorption spectrum of ketorolac computed at the CASPT2 and DFT computational levels in the gas phase or acetonitrile. Rendering that the lowest vertical absorption energies correspond to electronic excitations from the oxygen lone pair, of the carbonyl group, and the π orbitals the pyrrole and benzene to the

antibonding π* orbital of the C_3O_1 moiety [$^1(n_O \rightarrow \pi_{CO}^*)$, $^1(\pi_{Py} \rightarrow \pi_{CO}^*)$, and $^1(\pi_{Bz} \rightarrow \pi_{CO}^*)$, respectively]. In particular, a value of 3.85 eV is obtained at the CASPT2 level for the $^1(n_O \rightarrow \pi_{CO}^*)$ excitation in the gas phase, which follows from the $^1(\pi_{Py} \rightarrow \pi_{CO}^*)$, $^1(\pi_{Bz} \rightarrow \pi_{CO}^*)$, and a secondary $^1(\pi_{Py} \rightarrow \pi_{CO}^*)$ with energies of 4.46, 4.70 eV, and 4.76 eV, respectively. Similar calculations carried out in DFT result in lower energies with differences at most 0.30 eV, for the lowest $^1(\pi_{Py} \rightarrow \pi_{CO}^*)$ state. Additionally, solvent effect in the DFT method and PCM model showed small changes in the excitation energies, with a blue shift in the $^1(n_O \rightarrow \pi_{CO}^*)$ transition (0.10 eV larger) and red shifts of the $^1(\pi \rightarrow \pi_{CO}^*)$ excitation (lower values in the range 0.09-0.12 eV). In general, although $^1(n_O \rightarrow \pi_{CO}^*)$ requires the lowest excitation energy, this will be a dark transition in the absorption spectrum as expected from its lower oscillator strength (*f*). Thus, light absorption will mainly excite electrons from the π-system of the pyrrole ring to the antibonding π* orbital of the carbonyl group. Interestingly, both CASSCF/CASPT2 and DFT approaches in gas-phase render excitation energies in the range 4.16-4.46 eV (or 298-278 nm) for this state that increases to 4.04 eV (or 307 nm) in ACN (see Tables S2 and S3). Similar results are found in the DFT study of the absorption spectrum in the *trans* isomer of ketorolac (see Table S4), with excitation energies close to the values related to *cis*-ketorolac (energy differences no larger than 0.13 eV). According to these theoretical analyses, the lowest and brightest absorption band measured in the experiments (Figure S1) can be clearly related to the lowest $^1(\pi_{Py} \rightarrow \pi_{CO}^*)$ state.

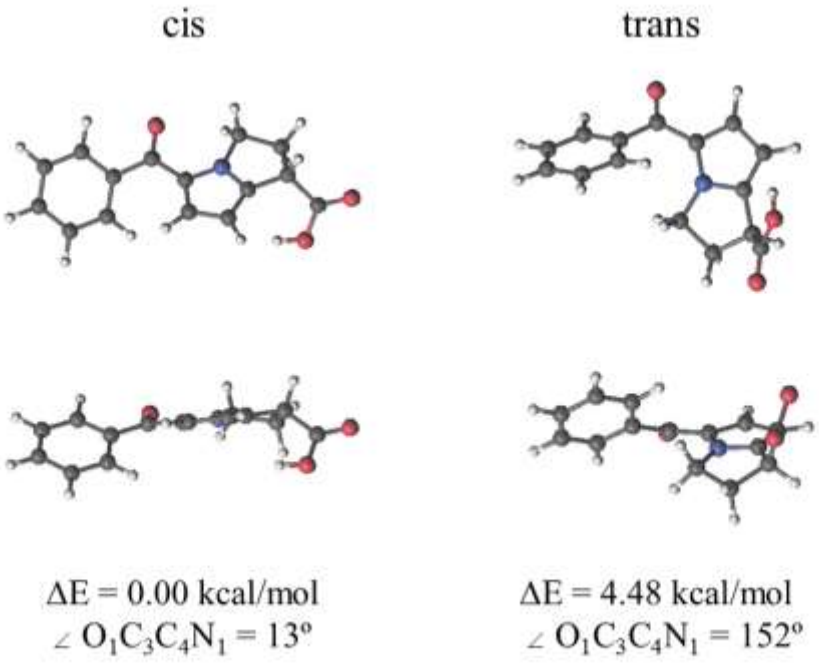

Figure S4. Stability analysis of the ground-state *cis* and *trans* ketorolac isomers in the gas phase. Structures (frontal and side views) and energies relative to the most stable isomer computed at the B3LYP/6-31G(*d*,*p*) level of theory.

Table S2. Calculated CASSCF/CASPT2 and DFT excitation energies (ΔE; eV, and nm in parenthesis) and oscillator strengths (*f*) for the singlet excited states in ketorolac.

State	CASPT2		DFT			
			In vacuo		Acetonitrile	
	ΔE	*f*	ΔE	*f*	ΔE	*f*
Singlet ($\pi\rightarrow\pi^*$) transitions						
$^1(\pi_{Py}\rightarrow\pi_{CO}^*)$	4.46 (278)	0.247	4.16 (298)	0.388	4.04 (307)	0.493
$^1(\pi_{Py}\rightarrow\pi_{CO}^*)$	4.76 (260)	0.191	4.54 (273)	0.011	4.45 (279)	0.024
$^1(\pi_{Bz}\rightarrow\pi_{CO}^*)$	4.70 (264)	0.012	4.62 (268)	0.020	4.52 (274)	0.014
Singlet ($n\rightarrow\pi^*$) transitions						
$^1(n_O\rightarrow\pi_{CO}^*)$	3.85 (322)	0.001	3.72 (333)	0.001	3.82 (325)	0.002

Table S3. Excitation energies (ΔE; eV, and nm in parenthesis) and oscillator strengths (*f*) for the cis-ketorolac lowest-lying singlet excited state $^1(\pi_{Py}\rightarrow\pi_{CO}^*)$ computed at different levels of theory.

Method	ΔE	*F*
	In vacuo	
B3LYP	4.16 (298)	0.388
CASPT2//CASSCF(12-in-12)	4.46 (278)	0.247
CASPT2//CASSCF(14-in-13)	4.45 (278)	0.175
CASPT2//CASSCF(16-in-14)	4.40 (282)	0.216
	Acetonitrile	
B3LYP	4.04 (307)	0.493

Table S4. Calculated B3LYP excitation energies (ΔE; eV, and nm in parenthesis) and oscillator strengths (*f*) in vacuo for the low-lying singlet excited state in the *cis* and *trans* isomers of ketorolac.

	cis		Trans	
	ΔE	*f*	ΔE	*F*
$^1(n_O\rightarrow\pi_{CO}^*)$	3.72 (333)	0.001	3.62 (342)	0.010
$^1(\pi_{Py}\rightarrow\pi_{CO}^*)$	4.16 (298)	0.388	4.03 (307)	0.234
$^1(\pi_{Py}\rightarrow\pi_{CO}^*)$	4.54 (273)	0.011	4.57 (271)	0.010
$^1(\pi_{Py}\rightarrow\pi_{CO}^*)$	4.62 (268)	0.020	4.66 (266)	0.017

Low-lying triplet states. Gas-phase CASPT2 computations of the lowest triplet excitations at the geometry of the ground-state minimum structure were assessed. Table S5 shows the presence of three triplet states very close in energy and below the excitation energy of the brightest singlet $^1(\pi_{Py}\rightarrow\pi_{CO}^*)$ state (cf. Table S2): a $^3(n_O\rightarrow\pi_{CO}^*)$ state at 3.57 eV and two $^3(\pi\rightarrow\pi_{CO}^*)$ states at 3.55 and 3.62 eV. According to the total dipole

moment (μ) analysis, these energies are not expected to change markedly since the μ values for these triplet states are very close and not far from the μ of the singlet ground state [μ (S_0)]. All three triplet states can in principle be populated along the deactivation path of the brightest singlet state by means of an intersystem-crossing process. The triplet $^3(n_O \rightarrow \pi_{CO}^*)$ will be however more favored taking into account the El-Sayed principle.[7]

Table S5. Calculated CASSCF/CASPT2 excitation energies (ΔE; eV, and nm) and total dipole moments (μ, in Debye) for the triplet excited states of ketorolac.

State	ΔE		μ^a
	eV	nm	
	Triplet ($\pi \rightarrow \pi^*$) transitions		
$^3(\pi_{Py} \rightarrow \pi_{CO}^*)$	3.55	348	3.81
$^3(\pi_{Bz} \rightarrow \pi_{Bz}^*)$	3.62	341	5.26
$^3(\pi_{Bz} \rightarrow \pi_{CO}^*)$	4.56	272	4.13
	Triplet ($n \rightarrow \pi^*$) transitions		
$^3(n_O \rightarrow \pi_{CO}^*)$	3.57	347	5.02

[a] μ (S_0) = 4.69 Debye.

The geometries of the two lowest lying triplet state at the Franck-Condon region, $^3(\pi_{Py} \rightarrow \pi_{CO}^*)$ and $^3(n_O \rightarrow \pi_{CO}^*)$, were optimized at the CASSCF level of theory. Thus, while the $^3(n_O \rightarrow \pi_{CO}^*)$ relaxed structure results in a large C_3O_1 bond of 1.36 Å (see Table S7), the $^3(\pi_{Py} \rightarrow \pi_{CO}^*)$ state evolves towards a delocalized excitation over the π system of the CO and pyrrole groups, $^3(\pi_{Py} \rightarrow \pi_{Py,CO}^*)$, and the main geometrical change corresponds to a butterfly movement of the two rings in the pyrrole (the dihedral angle $C_7N_1C_4C_8$ is found to be 127 degrees in the minimum structure of this state). Table S6 compiles the predicted phosphorescence emission for both $^3(\pi_{Py} \rightarrow \pi_{Py,CO}^*)$ and

$^3(n_O \rightarrow \pi_{CO}^*)$ states. Coincidently, the experimental observation (see Fig. S2) is consistent with the computed band maximum (E_{VE}) related to the $^3(n_O \rightarrow \pi_{CO}^*)$ state (E_{VE} = 2.60 eV). The emission from $^3(\pi_{Py} \rightarrow \pi_{Py,CO}^*)$ is found at lower energies (E_{VE} = 2.19 eV) and therefore might be relevant in the photophysics of ketorolac.

Table S6. Calculated CASSCF/CASPT2 emission energies (eV, and nm in parenthesis) for the low-lying triplet excited states for ketorolac in gas phase. Solvatochromic shifts in ACN, obtained from the analysis of the CASSCF dipole moments, are also indicated qualitatively (*srs* and *ns* states for small red-shift, and no shift, respectively)

	$0 \rightarrow 0^a$	$E_{VE}{}^b$
$^3(\pi_{Py} \rightarrow \pi_{Py,CO}^*)$	2.94 (420) *ns*	2.19 (564) *ns*
$^3(n_O \rightarrow \pi_{CO}^*)$	3.05 (406) *ns*	2.60 (477) *srs*

[a] $0 \rightarrow 0$ = beginning of the band, i.e., between the ground state geometry and the minimum of the excited state. [c] E_{VE} = emission maximum, from the excited state geometry vertically to the ground state.

Table S7. CASSCF(12-in-12)/ANO-S 321/21 calculated gas-phase most relevant geometrical parameters for the ground (gs) and the lowest-lying excited singlet [$^1(\pi_{Py} \rightarrow \pi_{CO}^*)$] and triplet [$^3(\pi_{Py} \rightarrow \pi_{Py,CO}^*)$ and $^3(n_O \rightarrow \pi_{CO}^*)$] states in *cis*-ketorolac. Bond lengths in Å and dihedral angles in degrees.

	gs	$^1(\pi_{Py} \rightarrow \pi_{CO}^*)$	$^3(\pi_{Py} \rightarrow \pi_{Py,CO}^*)$	$^3(n_O \rightarrow \pi_{CO}^*)$
C_2C_3	1.50	1.42	1.50	1.43
C_3O_1	1.21	1.27	1.22	1.36
C_3C_4	1.48	1.47	1.46	1.44
C_4C_5	1.39	1.47	1.47	1.39
C_5C_6	1.43	1.38	1.35	1.43
C_6C_7	1.37	1.41	1.49	1.38
N_1C_4	1.36	1.37	1.41	1.37
N_1C_7	1.37	1.32	1.43	1.36
$C_1C_2C_3O_1$	33	0	42	11
$O_1C_3C_4N_1$	17	80	8	33
$C_2C_3C_4C_5$	22	91	10	28
$C_7N_1C_4C_8$	174	173	127	175

Time resolved measurements: Ketorolac transient absorption spectra and kinetics were recorded with a LFP-111 laser-flash photolysis system (Luzchem Inc., Ottawa, Canada), using the fourth harmonic from a Surelite II, Nd-YAG laser (266 nm, *ca.* 10 ns, 8

mJ/pulse) as excitation source. The transient spectra were recorded using a 7x7 mm cell flow system (from Luzchem Inc.), averaging 3 laser shots at each wavelength. Ketorolac triplet quenching experiments were performed by using 1,4-cyclohexadiene, 2-propanol, tryptophan methyl ester, tyrosine methyl ester and 2'-deoxyguanosine as quenchers employing for excitation the third harmonic of a Nd-YAG laser (355 nm, *ca.* 10 ns, 8 mJ/pulse). The same setup was employed for energy transfer experiments from benzophenone triplet excited state. Singlet oxygen kinetic time profiles were measured by recording the singlet oxygen phosphorescence at 1270 nm, using a Hamamatsu NIR detector (peltier cooled at -62.8°C operating at 700 V, coupled to a grating monochromator) after laser excitation by a Surelite II, Nd-YAG laser (266 nm, *ca.* 10 ns, from up to 8 mJ/pulse). The data were acquired and processed with a customized Luzchem Research LFP-111 system. Primary data fitted well a monoexponential decay rendering the signal intensity at time zero for each different laser power excitation. From these data the singlet oxygen quantum yield was calculated according to Eq. 1.[8]

$$\Phi_{Ketorolac} = \Phi_{Phen} \frac{slope_{Ketorolac}}{slope_{Phen}} \qquad (1)$$

where $slope_{Ketorolac}$ and $slope_{Phen}$ correspond to the slopes from laser power dependence experiments. Φ_{Phen} corresponds to phenalenone singlet oxygen quantum yield ~ 1.0.[8]

Low temperature ketorolac triplet phosphorescence emission: The low temperature (77K) phosphorescence spectrum was recorded in EPA solution (ethyl ether:iso-pentane:ethanol mixture 5:5:2)[99] on a PTI model 100 spectrofluorometer, employing a pulsed Xenon lamp (λ_{exc}=300 nm) and a low-temperature accessory.

Photodecarboxylation quantum yield: Decarboxylation quantum yields were estimated from following the drug consumption by UV-Vis spectroscopy over time elicited from

sample exposure to a Xenon Lamp (Luzchem Inc., Ottawa, Canada) equipped with a water filter to prevent sample heating. Light absorbed doses were measured by using a SPR-4001 Spectroradiometer (Luzchem Inc., Ottawa, Canada); in all quantum yield calculations only initial slopes were considered in order to avoid sequential contribution of oxidation products produced during the irradiation.

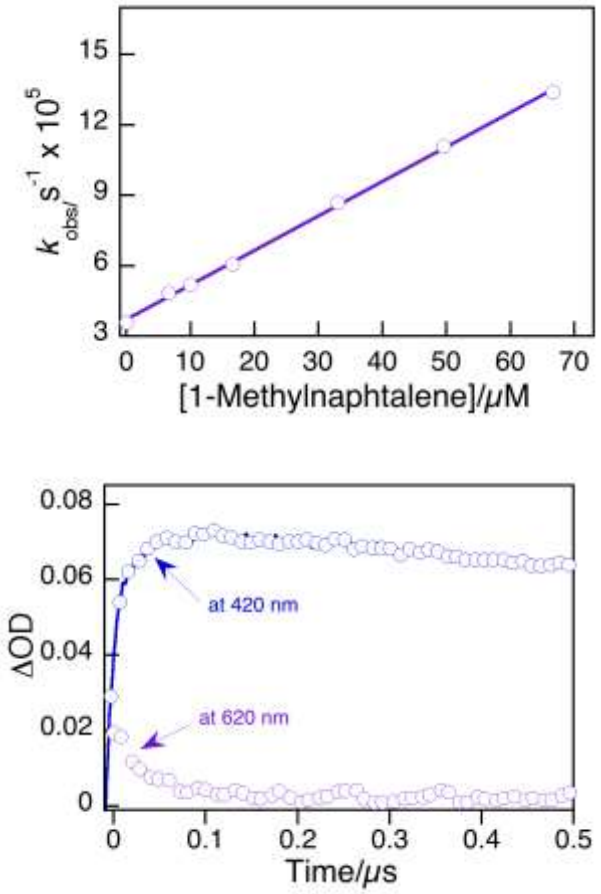

Figure S5. $1/k_{obs}$ at 620 nm as function of 1-methylnaphthalene concentration (**top**) and transient signal profile for ketorolac at 620 nm and 1-methylnaphthalene at 420 nm after laser excitation (bottom). All measurements were performed in deaerated acetonitrile at room temperature.

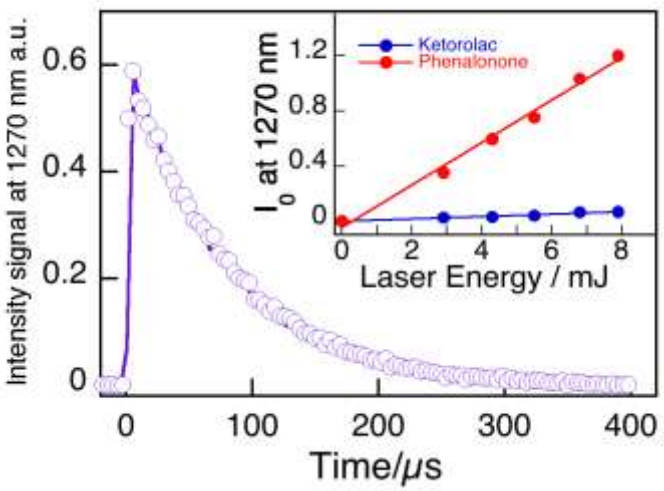

Figure S6. Singlet oxygen phosphorescence time profile at 1270 nm obtained after laser excitation at 266 nm. The inset shows the changes in initial signal at different laser powers for ketorolac (blue circles) or phenalenone (red circles). All measurements were performed in acetonitrile at room temperature.

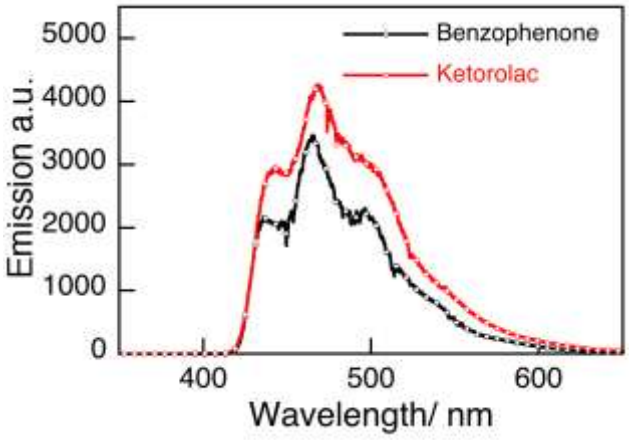

Figure S7. Ketorolac phosphorescence spectrum. Benzophenone phosporesecence spectrum has been added for comparison purposes.

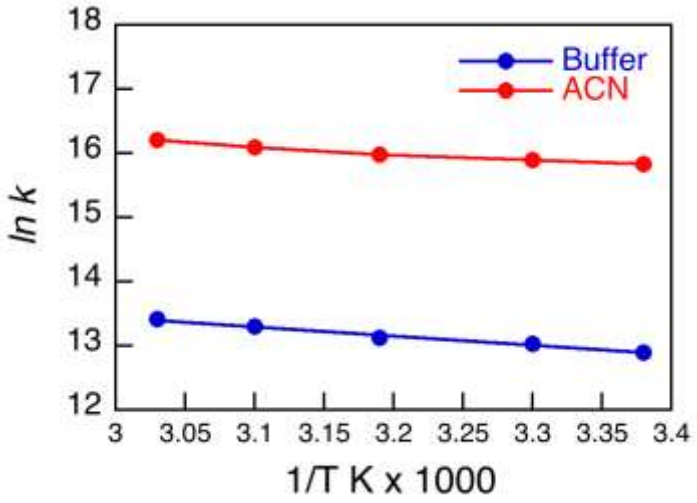

Figure S8. Dependence of natural logarithm of the rate constant for Ketorolac transient at 620 nm with the reciprocal of the temperature. In acetonitrile (red circles) or buffer pH 7.4 (blue circles) in nitrogen saturated solution. The relative error was less than 5% for all of them.

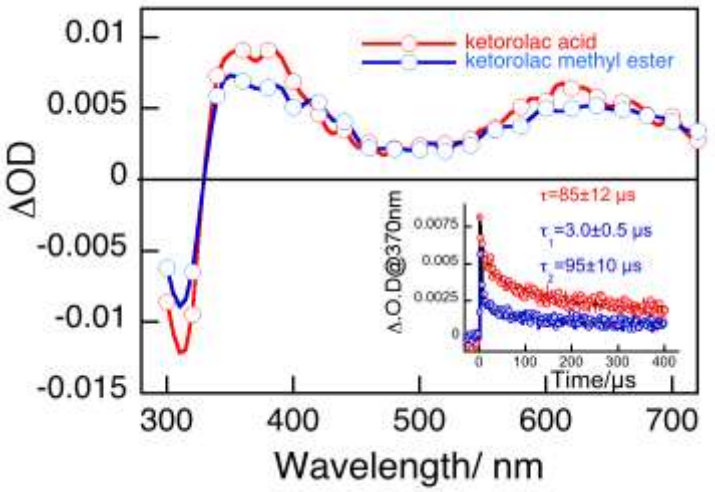

Figure S9. Transient absorption spectra for ketorolac acid (red circles) and ketorolac methyl ester (blue circles) obtained 1.0 μs after 266 nm laser excitation. Inset: ΔOD dependence at 370 nm. All measurements were performed in acetonitrile.

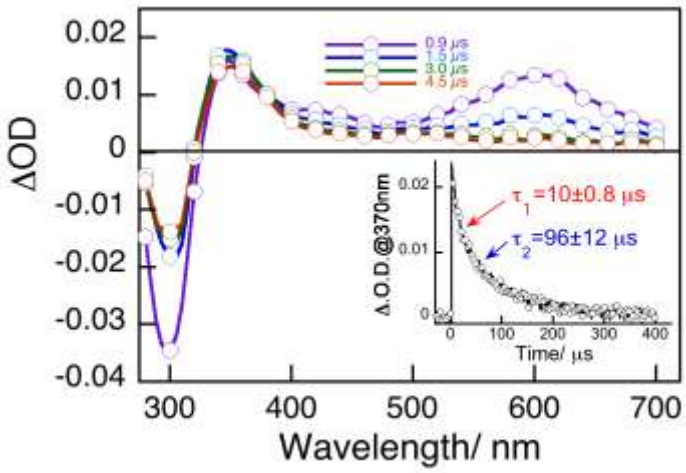

Figure S10. 2-Benzoylpyrrole transient absorption spectra obtained at 0.9, 1.5, 3.5 and 4.5 μs after 266 nm laser excitation under nitrogen. Inset: kinetic time profile monitored at 370 nm. All measurements were performed in acetonitrile at room temperature.

References

1. H. J. Doh, W. J. Cho, C. S. Yong, H. G. Choi, J. S. Kim, C. H. Lee and D. D. Kim, *J. Pharm. Sci.*, 2003, **92**, 1008-1017.
2. G. Cosa, L. Llauger, J. C. Scaiano and M. A. Miranda, *Org. Lett.*, 2002, **4**, 3083-3085.
3. L. Gu, H.-S. Chiang and D. Johnson, *Int. J. Pharm.*, 1988, **41**, 105-113.
4. M. J. Frisch, G. W. Trucks, H. B. Schlegel, G. E. Scuseria, M. A. Robb, J. R. Cheeseman, G. Scalmani, V. Barone, B. Mennucci, G. A. Petersson, H. Nakatsuji, M. Caricato, X. Li, H. P. Hratchian, A. F. Izmaylov, J. Bloino, G. Zheng, J. L. Sonnenberg, M. Hada, M. Ehara, K. Toyota, R. Fukuda, J. Hasegawa, M. Ishida, T. Nakajima, Y. Honda, O. Kitao, H. Nakai, T. Vreven, J. Montgomery, J. A., J. E. Peralta, F. Ogliaro, M. Bearpark, J. J. Heyd, E. Brothers, K. N. Kudin, V. N. Staroverov, R. Kobayashi, J. Normand, K. Raghavachari, A. Rendell, J. C. Burant, S. S. Iyengar, J. Tomasi, M. Cossi, N. Rega, N. J. Millam, M. Klene, J. E. Knox, J. B. Cross, V. Bakken, C. Adamo, J. Jaramillo, R. Gomperts, R. E. Stratmann, O. Yazyev, A. J. Austin, R. Cammi, C. Pomelli, J. W. Ochterski, R. L. Martin, K. Morokuma, V. G. Zakrzewski, G. A. Voth, P. Salvador, J. J. Dannenberg, S. Dapprich, A. D. Daniels, Ö. Farkas, J. B. Foresman, J. V. Ortiz, J. Cioslowski and D. J. Fox, 2009.
5. F. Aquilante, L. De Vico, N. Ferré, G. Ghigo, P.-Å. Malmqvist, P. Neogrády, T. B. Pedersen, M. Pitoňák, M. Reiher, B. O. Roos, L. Serrano-Andrés, M. Urban, V. Veryazov and R. J. Lindh, *J. Comput. Chem.*, 2010, **31**, 224-227.
6. B. O. Roos, R. Lindh, P.-Å. Malmqvist, V. Veryazov and P.-O. Widmark, *J. Phys. Chem. A.*, 2004, **108**, 2851-2858.
7. N. J. Turro, V. Ramamurthy and J. C. Scaiano, *Principles of molecular photochemistry*, University Science Books, Sausalito, California, 2009.

8. S. Nonell and S. E. Braslavsky, *Meth. Enzymol.*, 2000, **319**, 37-49.
9. S. L. Murov, I. Carmichael and G. L. Hug, *Handbook of photochemistry*, Mercel Decker Inc, New York, 1993.